Chapter 6 | Wind Distribution in the PBL

6.1 Factors Influencing Wind Distribution

The magnitude and direction of near-surface winds and their variations with height in the PBL are of considerable interest to micrometeorologists. The following factors influence the wind distribution in the PBL:

- Large-scale horizontal pressure and temperature gradients in the lower atmosphere, which drive the PBL flow.
- The surface roughness characteristics, which determine the surface drag and momentum exchange in the lower part of the PBL.
- The earth's rotation, which makes wind turn with height.
- The diurnal cycle of heating and cooling of the surface, which determines the thermal stratification of the PBL.
- The PBL depth, which determines wind shears in the PBL.
- Entrainment of the free atmospheric air into the PBL, which determines the momentum, heat, and moisture exchanges at the top of the PBL, as well as the PBL height.
- Horizontal advections of momentum and heat, which affect both the wind and temperature distributions in the PBL.
- Large-scale horizontal convergence or divergence and the resulting mean vertical motion at the top of the PBL.
- Presence of clouds and precipitation in the PBL, which influence its thermal stratification.
- Surface topographical features, which give rise to local or mesoscale circulations.

Some of these factors will be discussed in more detail in the following text, while others are considered outside the scope of this introductory text.

6.2 Geostrophic and Thermal Winds

The PBL is essentially driven by large-scale atmospheric motions which are set up in response to spatial variations of air pressure and temperature. The geostrophic winds are related to or defined in terms of the pressure gradients as

$$U_g = -\frac{1}{\rho f}\frac{\partial P}{\partial y}; \quad V_g = \frac{1}{\rho f}\frac{\partial P}{\partial x} \tag{6.1}$$

in which U_g and V_g are the components of geostrophic wind vector **G** in the x and y directions, respectively, and f is the Coriolis parameter, which is related to the rotational speed of the earth (Ω) and latitude (ϕ) as

$$f = 2\Omega \sin \phi \tag{6.2}$$

The geostrophic winds are the winds which would occur as a result of the simple geostrophic balance between the pressure gradient and Coriolis (rotational) forces in a frictionless atmosphere with no advective and local accelerations. Equation (6.1) implies that **G** must be parallel to the isobars with low pressure to the left in the northern hemisphere ($f > 0$) (see Figure 6.1) and low pressure to the right in the southern hemisphere ($f < 0$). The absence of advective accelerations further implies that, locally, isobars are equispaced, parallel, straight lines. The geostrophic balance is often assumed to occur, i.e., $U = U_g$ and $V = V_g$, at the top of and outside the PBL. Within the PBL, however, actual

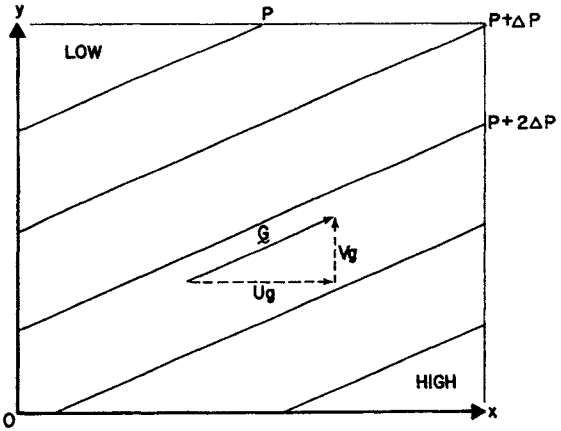

Figure 6.1 Schematic of relationship between geostrophic winds and isobars for the northern hemisphere.

winds differ from the geostrophic winds because of the surface friction and the vertical exchange of momentum.

The horizontal pressure gradients or geostrophic winds may vary with height in response to horizontal temperature gradients. The vertical gradients of geostrophic winds, i.e., geostrophic wind shears, are given by the thermal wind equations

$$\frac{\partial U_g}{\partial z} = -\frac{g}{fT}\frac{\partial T}{\partial y} + \frac{U_g}{T}\frac{\partial T}{\partial z} \cong -\frac{g}{fT}\frac{\partial T}{\partial y}$$
$$\frac{\partial V_g}{\partial z} = \frac{g}{fT}\frac{\partial T}{\partial x} + \frac{V_g}{T}\frac{\partial T}{\partial z} \cong \frac{g}{fT}\frac{\partial T}{\partial x} \tag{6.3}$$

which can be derived from Equation (6.1) in conjunction with the hydrostatic equation and the equation of state (Hess, 1959, Chapter 12). The approximations on the right-hand side of Equation (6.3) ignore the stability-dependent terms, which may account for no more than 10% variation in geostrophic winds per kilometer of height. The approximate thermal wind equations imply that the geostrophic wind shear vector $\partial \mathbf{G}/\partial z$ must be parallel to the isotherms with colder air to the left in the northern hemisphere (Figure 6.2). A part of the geostrophic wind shear is due to the normal (climatological) decrease of temperature in going toward the poles, while a substantial part may be due to local temperature gradients created by surface topographical features (e.g., land–sea, urban–rural, and mountain–valley contrasts) and/or the synoptic weather situation. Note that a horizontal temperature gradient of only 1°C per 100 km will cause a geostrophic wind shear of about 3.3 m s^{-1} km^{-1} or 0.0033 s^{-1} in middle latitudes.

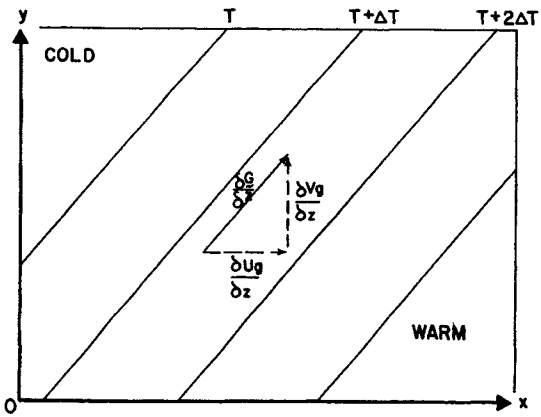

Figure 6.2 Schematic of relationship between thermal winds or geostrophic shears and isotherms for the northern hemisphere.

The changes in geostrophic wind components over a given layer depth, Δz, can be calculated from the finite-difference form of Equation (6.3):

$$\Delta U_g = -\frac{\Delta z g}{fT}\frac{\partial T}{\partial y}; \quad \Delta V_g = \frac{\Delta z g}{fT}\frac{\partial T}{\partial x} \tag{6.4}$$

Horizontal temperature gradients or geostrophic shears are generally assumed to be constant (independent of height) in the PBL. It follows from Equation (6.3) or (6.4) that geostrophic winds must vary with height in the presence of finite temperature gradients. Figure 6.3 illustrates for the northern hemisphere the relationship between the geostrophic winds at the surface and the top of the PBL (taking $\Delta z = h$) for different orientations of the surface geostrophic wind

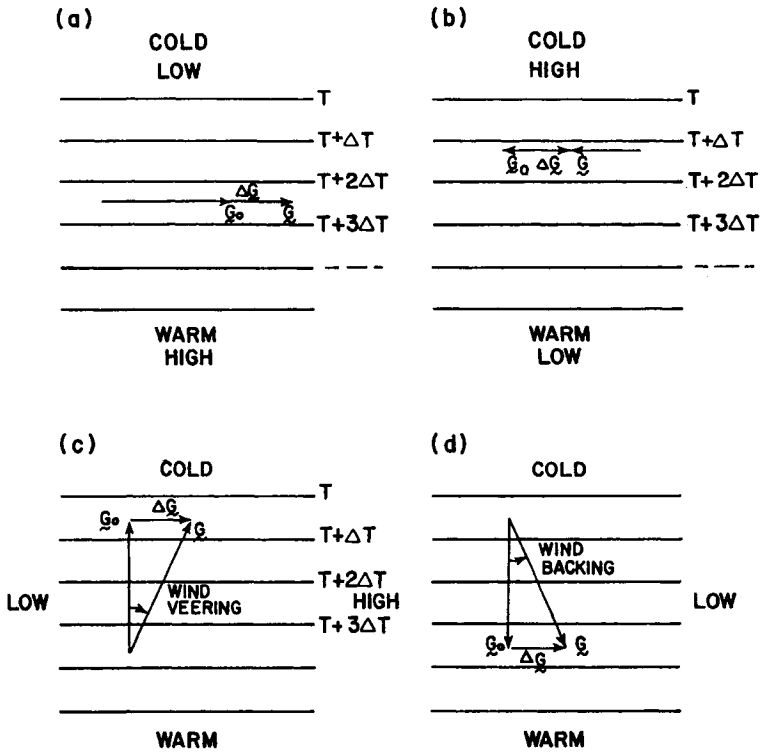

Figure 6.3 Schematic of the relationship between the geostrophic winds at the surface and the top of the PBL for different orientations of surface isobars or $\mathbf{G}_0$ and surface isotherms: (a) parallel geostrophic flow around a 'cold low' or a 'warm high'; (b) parallel flow around a 'cold high', or a 'warm low'; (c) veering geostrophic flow in warm advection; (d) backing flow in cold advection.

$\mathbf{G}_0$ with respect to the isotherms. Again, isobars and isotherms are taken as parallel straight lines for the ideal case of no advective acceleration.

Note that when $\mathbf{G}_0$ is parallel to the isotherms (no temperature advection), the effect of the horizontal temperature gradient is to increase or decrease the magnitude of geostrophic winds, without causing any change in the direction. This will be the rare situation when isobars are parallel to the isotherms throughout the layer. In general, however, the surface isobars are not parallel to the isotherms and the surface geostrophic wind has a component from cold toward warm temperatures or vice versa. Such a flow tends to change the vertical temperature distribution due to horizontal advection of cold or warm air. Figure 6.3 shows that both the magnitude and the direction of the geostrophic wind may change with height in the presence of heat advection. The geostrophic wind turns cyclonically (backs) with height in the case of cold air advection, and it turns anticyclonically (veers) with height in the case of warm advection. Actual winds within the PBL may also be expected to back or veer with height in response to the backing and veering of geostrophic winds.

Equations (6.1) and (6.4) express the geostrophic and thermal winds in terms of horizontal pressure and temperature gradients on a horizontal (constant-level) surface. These can be used with the information provided on a surface chart depicting isobars and isotherms. The geostrophic and thermal winds in meteorology are often expressed in terms of the heights (z_p) of constant-pressure surfaces which are represented on upper-air (e.g., 850 mb, 700 mb, etc.) charts. On any constant-pressure surface, the geostrophic and thermal winds can be expressed as

$$U_g = -\frac{g}{f}\frac{\partial z_p}{\partial y}; \quad V_g = \frac{g}{f}\frac{\partial z_p}{\partial x} \tag{6.5}$$

$$\Delta U_g = -\frac{g}{f}\frac{\partial(\Delta z_p)}{\partial y}; \quad \Delta V_g = \frac{g}{f}\frac{\partial(\Delta z_p)}{\partial x} \tag{6.6}$$

where Δz_p is the thickness of the layer between the p_1 and p_2 constant-pressure surfaces and ΔU_g and ΔV_g are the corresponding thermal wind components. The hypsometric equation can be used to express Δz_p in terms of p_1 and p_2, and the average temperature of the layer. Equation (6.5) implies that the geostrophic wind is proportional to the slope of the constant-pressure surface.

The atmosphere is called barotropic, when there are no geostrophic shears or horizontal temperature gradients, and baroclinic, when there are significant geostrophic shears. In the same way, atmospheric boundary layers may be classified as barotropic and baroclinic PBLs. The term baroclinicity (or baroclinity) is often used as a synonym for geostrophic wind shear. It is not

difficult to see that the presence of geostrophic shears or baroclinity in the PBL is more a rule than the exception.

In strongly curved flows about low- and high-pressure systems, the centripetal force alters the normal geostrophic balance between pressure gradient and Coriolis forces. Consequently, the actual wind can be significantly more or less than the geostrophic wind in strongly cyclonic or anticyclonic flows. The so-called 'gradient wind' provides a much better approximation to the actual winds in strongly curved flow systems (Hess, 1959, Chapter 12; Holton, 1992, Chapter 3).

Example Problem 1

Surface isobars at a 30°N latitude site during a mid-day period run east–west, indicating a horizontal pressure gradient of 3 mb per 100 km toward the south. At this time, surface isotherms are nearly perpendicular to isobars indicating a horizontal temperature gradient of 1.5°C per 100 km toward the west. A temperature sounding indicated the PBL height of 2000 m and a temperature drop of 25°C across the PBL from the near-surface temperature of 35°C. The observed surface pressure is 1020 mb. Calculate the geostrophic winds (both magnitude and direction) at (a) the surface and (b) top of the PBL.

Solution

The Coriolis parameter for the site is given by

$$f = 2\Omega \sin\phi = 2 \times \frac{2\pi}{24 \times 3600} \times \sin 30^\circ \cong 0.73 \times 10^{-4}\ \mathrm{s}^{-1}$$

Air density near the surface can be determined from the equation of state

$$\rho = \frac{P}{RT} = \frac{1020 \times 10^2}{287.04 \times 308.2} \cong 1.15\ \mathrm{kg\ m}^{-3}$$

(a) In order to calculate the surface geostrophic wind from the observed pressure gradient, we use a geographical coordinate system with the x axis pointed toward the east and the y axis toward the north. In this coordinate system,

$$\frac{\partial P}{\partial x} = 0; \quad \frac{\partial P}{\partial y} = -3 \times 10^{-5}\ \mathrm{mb\ m}^{-1} = -3 \times 10^{-3}\ \mathrm{Pa\ m}^{-1}$$

Therefore

$$V_g = 0; \quad U_g = -\frac{1}{\rho f}\frac{\partial P}{\partial y} = \frac{10^4}{1.15 \times 0.73} \times 3 \times 10^{-3}$$

$$\cong 35.74 \text{ ms}^{-1}$$

Thus, the magnitude of the surface geostrophic wind, $G_0 = 35.74$ m s^{-1}, and its direction is from the west (270°).

(b) Before calculating the geostrophic wind at the top of the PBL ($h = 2000$ m), we need to calculate the thermal wind components from Equation (6.4) with $\Delta z = h = 2000$ m. From the observations, we have

$$\frac{\partial T}{\partial x} = -1.5 \times 10^{-5} \text{ K m}^{-1}; \quad \frac{\partial T}{\partial y} = 0$$

The average temperature in the PBL, $T = 295.7$ K.
Thus,

$$\Delta V_g = \frac{hg}{fT}\frac{\partial T}{\partial x} \cong 13.63 \text{ m s}^{-1}; \quad \Delta U_g = 0$$

Then, the geostrophic wind components at the top of the PBL can be determined as

$$U_{gh} = U_{g0} + \Delta U_g = 35.74 \text{ m s}^{-1}$$

$$V_{gh} = V_{g0} + \Delta V_g = -13.63 \text{ m s}^{-1}$$

Therefore, the magnitude of the geostrophic wind,

$$G_h = [(35.74)^2 + (13.63)^2]^{1/2} \cong 38.25 \text{ m s}^{-1}$$

and its direction is 291° (NW).

6.3 Friction Effects on the Balance of Forces

Because air is a viscous fluid, its velocity relative to the earth's surface must vanish right at the surface. This does not happen abruptly, but the retarding influence of the surface on atmospheric winds pervades the whole depth of the PBL. Consequently, the wind speed decreases gradually and the mean momen-

tum is transferred downward in going toward the surface. Turbulence provides an efficient mechanism for the transfer of momentum from one level to another in the vertical. Also, vertical exchange of horizontal momentum results in the so-called frictional force on any fluid element. Because of this, the simple geostrophic balance between the pressure gradient and Coriolis forces, which may exist outside the PBL, cannot be expected to occur within the PBL.

Figure 6.4 is a schematic of the balance of pressure gradient, Coriolis, and friction forces on fluid elements at different levels in a barotropic PBL. The corresponding geostrophic and actual wind vectors are also shown with the stipulation that the Coriolis force must always be normal to V and proportional to wind speed, while the friction force must be perpendicular to the ageostrophic wind vector (V − G). These conditions follow from the equation of mean motion in the absence of local and advective accelerations.

$$2\rho\Omega \times (\mathbf{V} - \mathbf{G}) = \partial\tau/\partial z \tag{6.7}$$

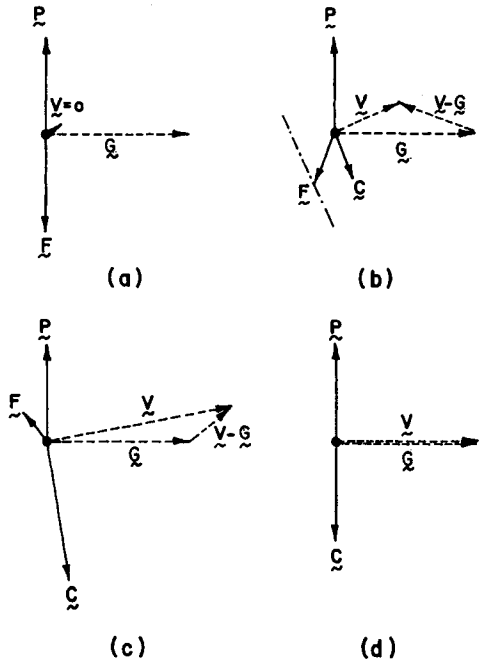

Figure 6.4 Schematic of the balance of forces on a fluid parcel at different heights in a barotropic PBL: (a) at the surface; (b) in the surface layer; (c) in the middle of the PBL; (d) at the top of the PBL. Actual and geostrophic velocities are also indicated. [After Arya (1986).]

Note that in a rotating frame of reference or in the presence of directional shear, the friction force on a fluid element need not be parallel and opposite to the velocity vector, as commonly depicted in many textbook schematics of the force balance in the friction layer. Figure 6.4a shows that, right at the surface where the Coriolis force disappears, the friction force must exactly balance the pressure gradient force and, hence, make a large angle with the direction of near-surface wind or surface shear. As wind speed increases with height, with little change in the wind direction through the surface layer, the balance of forces requires that the friction force decreases and rotates anticyclonically with increasing height (Figure 6.4b). The same tendency continues through the outer part of the PBL also, as wind veers and increases in magnitude (it often becomes super-geostrophic in the middle of the PBL), as shown in Figure 6.4c. Near the top of the PBL, the friction force becomes small in magnitude and highly variable in direction, in response to the changes in the direction of $\mathbf{V} - \mathbf{G}$, as velocity oscillates about the geostrophic equilibrium. Ignoring any such oscillations, as well as any inertial oscillations that may be present in the real atmosphere, the force balance at the top of the PBL is depicted in Figure 6.4d.

The above considerations of the balance of forces suggest that winds must veer with height in a barotropic PBL. The difference between the wind direction at some height and that near the surface is called the veering angle, which normally increases with height in a barotropic PBL. In the presence of thermal winds (geostrophic wind shear), however, actual winds may veer or back with increasing height, in response to the veering or backing of geostrophic winds and the frictional veering. In practice, frictional veering may be estimated as the difference between the actual wind veering and the geostrophic veering.

The angle between the directions of geostrophic and actual winds is called the cross-isobar angle (α) of the flow, which normally decreases with height and vanishes at the top of the PBL (assuming that geostrophic balance occurs there). The surface cross-isobar angle (α_0) which near-surface winds make with surface isobars is of considerable interest to meteorologists. It is found to depend on the surface roughness, latitude, and the surface geostrophic wind, as well as on the stability, baroclinity, and height of the PBL. For the neutral, barotropic PBL in middle and high latitudes, α_0 is found to range from about 10° for relatively smooth (e.g., water, ice, and snow) surfaces to about 35° for very rough (e.g., forests and urban areas) surfaces. It increases with increasing stability and decreasing latitude, so that a wide range of $\alpha_0 \cong 0$–45° occur in the stratified barotropic PBL. In the presence of thermal winds (baroclinic PBL), the range of observed surface cross-isobar angles becomes wider (say, -20 to 70°). Under certain conditions of strong baroclinity, α_0 may even become negative, implying that a component of the near-surface winds is directed toward the surface 'high' (Arya and Wyngaard, 1975; Arya, 1978).

Example Problem 2

The following observations are for a midlatitude ($f = 10^{-4}$ s^{-1}) PBL during the afternoon convective conditions:

Height (m)	10	100	1000	1500
Wind speed (m s^{-1})	9.0	15.5	17.0	15.0
Wind direction (deg.):	250	253	258	260

The PBL height = 1500 m.
The surface geostrophic wind speed = 20.0 m s^{-1}.
The surface geostrophic wind direction = 275°.

(a) Calculate the average magnitudes of the geostrophic wind shear and the actual wind shear in the PBL, assuming geostrophic balance at the top of the PBL.
(b) Estimate the total wind veering and the frictional veering across the PBL, as well as the cross-isobar angle of the near-surface winds.
(c) Compute the pressure gradient, Coriolis, and friction forces per unit mass at the 10 m level and show the force balance at this level.

Solution

(a) Using the geographical coordinate system with the x-axis pointed toward the east and the y-axis toward the north, the horizontal components of geostrophic winds at the surface and the top (h = 1500 m) of the PBL are:

$$U_{g0} = G_0 \cos(270 - 275) = 19.92 \text{ m s}^{-1}$$
$$V_{g0} = G_0 \sin(270 - 275) = -1.74 \text{ m s}^{-1}$$
$$U_{gh} = G_h \cos(270 - 260) = 14.77 \text{ m s}^{-1}$$
$$V_{gh} = G_h \sin(270 - 260) = 2.60 \text{ m s}^{-1}$$

The components of the geostrophic wind shear across the PBL can, then, be calculated as

$$\Delta U_g = 14.77 - 19.92 = -5.15 \text{ m s}^{-1}$$
$$\Delta V_g = 2.60 - (-1.74) = 4.34 \text{ m s}^{-1}$$
So that, $|\Delta \mathbf{G}| = [(5.15)^2 + (4.34)^2]^{1/2} = 6.73 \text{ m s}^{-1}$

The magnitude of the geostrophic wind shear across the PBL = $|\Delta \mathbf{G}|/h \cong 4.49 \times 10^{-3}$ s^{-1}.
The average magnitude of the actual wind shear

$$\frac{|\mathbf{V}_h|}{h} = 10^{-2} \text{ s}^{-1}$$

(b) The total (actual) wind veering = 260 − 250 = 10°.
The geostrophic wind veering = 260 − 275 = −15°.

Frictional veering = total veering − geostrophic veering
= 10 − (−15) = 25°

The cross-isobar angle of near-surface winds = 275 − 250 = 25°, which is equal to the frictional veering across the PBL.

(c) The various forces per unit mass or accelerations are given as follows:

Type of force	Magnitude	Direction
Pressure gradient (**P**)	$f\|\mathbf{G}\|$	Normal to **G** oriented to the left of **G**
Coriolis force (**C**)	$f\|\mathbf{V}\|$	Normal to **V** oriented to the right of **V**
Friction force (**F**)	$f\|\mathbf{V} - \mathbf{G}\|$	Normal to (**V** − **G**)

In the absence of any local or advective acceleration, the above forces must balance, so that, at any height, $\mathbf{P} + \mathbf{C} + \mathbf{F} = 0$.
The magnitudes of the various forces at the 10 m level are:

$$|\mathbf{P}| = f|\mathbf{G}| = 2.0 \times 10^{-3}\ \mathrm{m\ s^{-2}}$$

$$|\mathbf{C}| = f|\mathbf{V}| = 0.9 \times 10^{-3}\ \mathrm{m\ s^{-2}}$$

$$|\mathbf{F}| = f|\mathbf{V} - \mathbf{G}| = 1.24 \times 10^{-3}\ \mathrm{m\ s^{-2}}$$

Note that $|\mathbf{V} - \mathbf{G}] \neq |\mathbf{V}| - |\mathbf{G}|$ but

$$|\mathbf{V} - \mathbf{G}] = [(U - U_g)^2 + (V - V_g)^2]^{1/2}$$

The force balance can easily be shown in a vector plot similar to Figure 6.4(b), knowing the magnitudes and directions of geostrophic and actual winds.

6.4 Stability Effects on the PBL Winds

We have discussed earlier how the diurnal cycle of heating and cooling of the surface, in conjunction with radiative, convective, and advective processes occurring within the PBL, determine the static or thermal stability of the PBL. Through its strong influence on the vertical movements of air parcels, thermal stability strongly influences the vertical exchange of momentum and, hence, the wind distribution in the PBL.

On a clear day the surface warms up relative to the air above, in response to solar heating. This gives rise to a variety of convective circulations, such as near-surface plumes, thermals (updrafts) and downdrafts, which can directly transfer momentum and heat in the vertical direction. The upward transfer of heat through the lower part of the PBL is largely responsible for convective or buoyancy-generated turbulence. The resulting vigorous mixing of momentum leads to considerable weakening and, sometimes, elimination of mean wind shears in the PBL. Thus, it is not uncommon to find nearly uniform wind speed and wind direction profiles through much of the daytime convective boundary layer (CBL). Strong wind shears are largely confined to the lower part of the surface layer and the shallow transition layer near the base of inversion which often caps the convective mixed layer. Changes in mean wind direction between the surface and the inversion base are typically less than 20°.

On a clear evening and night, on the other hand, the surface cools down in response to longwave radiation and a surface inversion begins to form and develop. Since buoyancy inhibits vertical momentum exchanges in the inversion layer, significant wind speed and direction shears develop in this layer. Wind direction changes of 30° or more across the shallow stable boundary layer (SBL), which may comprise only a part of the surface inversion layer, are not uncommon. The wind speed profile is generally characterized by a low-level jet in which winds are often supergeostrophic. The winds in the outer part of the SBL may undergo inertial oscillations in response to the inertially oscillating geostrophic flow. Internal gravity waves may also develop in such a stratified environment; such waves frequently appear mixed with turbulence.

Thermal stability also has a strong influence on the PBL height, which, in turn, affects the wind distribution. In the morning hours following sunrise, the PBL grows rapidly at first, in response to heating from below. This growth continues throughout the day, although at a progressively decreasing rate, resulting in a 1- to 2-km-deep mixed layer by mid-afternoon. Immediately following the evening transition period, when the sensible heat flux at the surface changes sign, the unstable PBL suddenly collapses and is replaced by a much shallower stable boundary layer. For a given wind speed at the top of the PBL, one would expect the average wind shear in the PBL to be an order of magnitude larger at night than that during the midday period, because of the difference in the PBL heights. Very close to the surface, however, wind shears are generally larger during the daytime than they are at night.

In the presence of wind shear, a dynamic stability parameter such as the gradient Richardson number

$$\mathrm{Ri} = \frac{g}{T_v}\frac{\partial \Theta_v}{\partial z}\left|\frac{\partial \mathbf{V}}{\partial z}\right|^{-2} \tag{6.8}$$

is considered to be a more appropriate stability parameter than the static stability parameter $s = (g/T_v)(\partial\Theta_v/\partial z)$ introduced earlier. Ri is dimensionless and has the same sign as s. It will be shown in Chapter 8 that the Richardson number is a better measure of the intensity of mixing (turbulence) and provides a simple criterion for the existence or nonexistence of turbulence in a stably stratified environment (a large positive value of $\mathrm{Ri} > 0.25$ is indicative of weak and decaying turbulence or a completely nonturbulent environment). Therefore, the vertical distribution of Ri may be used to determine the vertical extent of the boundary layer when other, more direct, measurements of the PBL height are not available.

6.5 Observed Wind Profiles

A considerable amount of wind profile data have been collected by meteorologists in the course of a number of large and small field experiments (Garratt and Hicks, 1990; Tunick, 1999), as well as from routine upper air soundings. Observations are made using pilot balloons, rawindsondes, tethersondes, doppler radars, acoustic sounders (sodars), instrumented aircraft, and tall towers. Consequently, scientists have developed a good understanding of the effects of surface roughness and stability on wind distribution in the PBL and a fair understanding of the influence of baroclinity on the same. More complicated effects of entrainment, advection, complex topography, clouds, and precipitation have received little attention from boundary layer meteorologists and remain poorly understood. The underlying philosophy in micrometeorology has been to study simple situations first in order to have a better understanding of the basic phenomena and then include progressively more complicating factors. Unfortunately, difficulties of measuring and computing turbulence in the atmospheric boundary layer have restricted micrometeorologists for a long time to the study of the more or less idealized (horizontally homogeneous, stationary, nonentraining, dry, etc.) PBL. Only recently have efforts been made to study the effects of complicating factors which influence the real-world PBL.

First, we present a few selected wind profiles for the 'ideal' PBL, taken under different stability conditions, in order to illustrate some qualitative effects of stability. Figure 6.5 shows the pibal wind and potential temperature profiles under fairly convective conditions during day 33 of the Wangara Experiment in southern Australia. Here, U and V are the horizontal wind components in the x and y directions, respectively, with the x axis parallel to the direction of near-surface winds and the y axis normal to the same (this choice of coordinate axes is more commonly used in micrometeorology than the geographical coordinate system, which is used in other branches of meteorology).

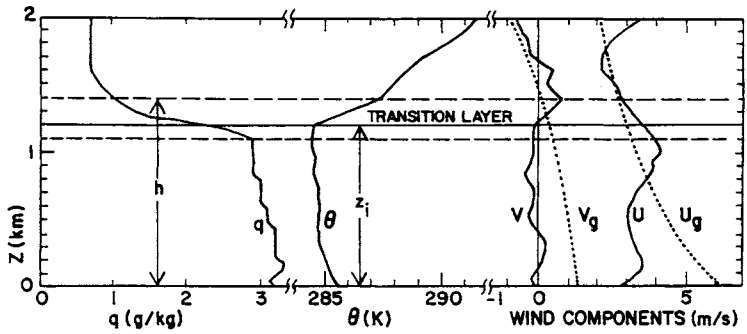

Figure 6.5 Measured wind, potential temperature and specific humidity profiles in the PBL under convective conditions on day 33 of the Wangara Experiment. [From Deardorff (1978).]

Note that despite the large geostrophic shear present on this day, wind profiles show the characteristic features of nearly uniform distributions in the convective mixed layer (the undulations in the PBL are probably caused by large eddies and organized updraft and downdraft motions whose effects are not smoothed out in pibal soundings), and strong gradients in the surface layer below and the transition layer above. Similar features have been observed in convective boundary layers over other homogeneous land and ocean surfaces (Figure 6.6a).

The observed mean wind and virtual potential temperature profiles under moderately unstable conditions in a trade wind marine PBL are shown in Figure 6.6b. At the time of these observations widely scattered shallow convective clouds were present whose bases coincided with the inversion base. Note that although the Θ_v profile is uniform throughout the subcloud layer, the wind profiles show significant shears in this layer. Still, the total wind veering across the unstable PBL remains small (about 8°), due to the combined effects of mechanical and buoyant mixing, smooth ocean surface, and low latitude.

The theoretician's ideal of a steady state, neutral, barotropic PBL is so rare in the atmosphere that relevant observations of the same do not exist. The wind profiles taken under slightly unstable and slightly stable conditions during the morning and evening transition hours differ considerably, due to the effects of nonstationarity and even slight stability or instability. An average of profiles taken during completely overcast and very windy conditions over sea might be more representative of a neutral PBL (Nicholls, 1985).

From observations of the nocturnal stable boundary layer (SBL), one can perhaps distinguish between the two broad stability regimes: (1) the moderately stable regime in which turbulent exchanges are more or less continuous in time and space through at least the lower half of the SBL; and (2) the very stable

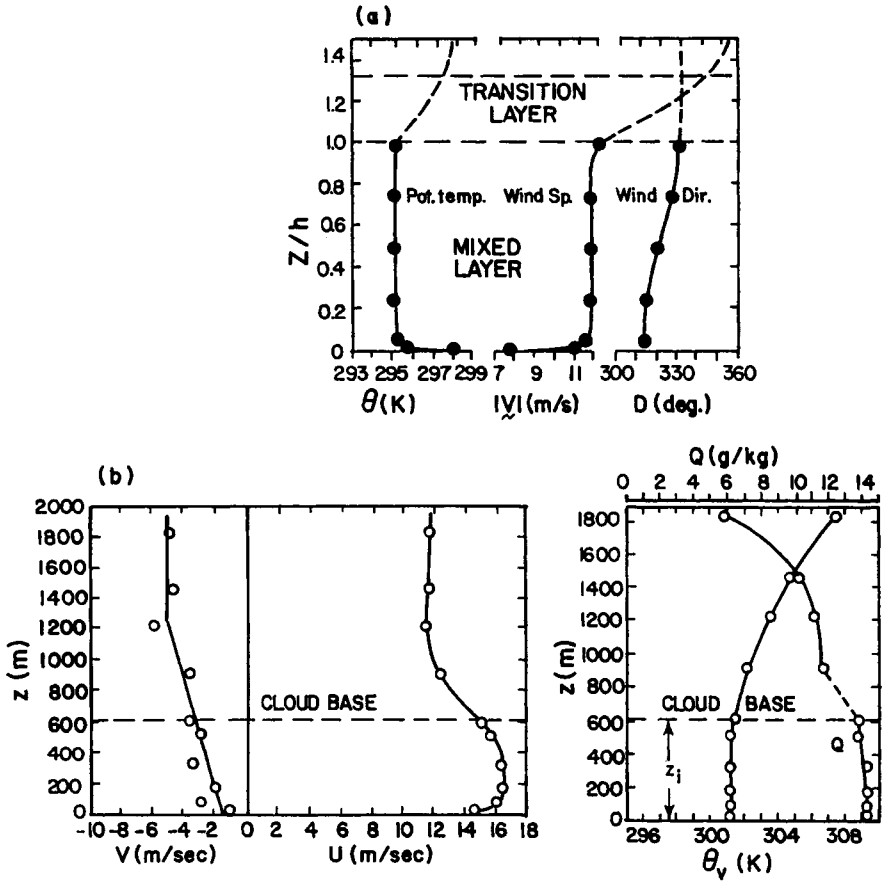

Figure 6.6 Observed vertical profiles of mean wind components, or wind speed and direction, potential temperature and specific humidity in the PBL. (a) Convective conditions overland. [After Kaimal *et al.* (1976).] (b) Unstable conditions over the ocean. [After Pennell and LeMone (1974).]

regime in which turbulent exchanges occur only intermittently in time and space through most of the SBL. The former can exist over land at night only during strong winds, and more likely at sea when the air is slightly warmer than the sea surface. The typical profiles of wind, potential temperature, and Richardson number in this moderately stable boundary layer are shown in Figure 6.7. These are based on the measurements from a tall tower near Dallas, Texas. Note that the U profile shows a pronounced maximum. The nose of the low-level jet often coincides with the top of the SBL, since it also represents the level of maximum

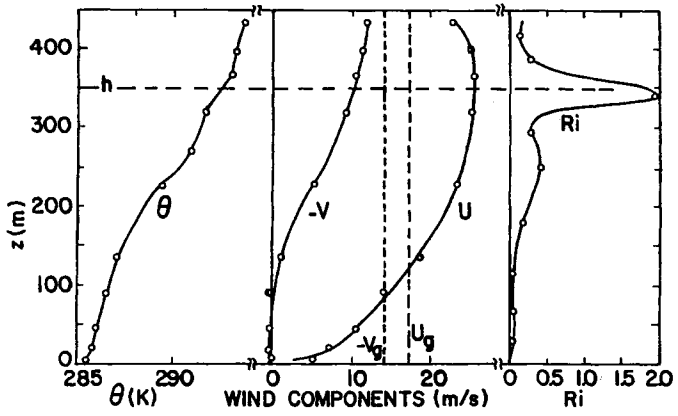

Figure 6.7 Observed vertical profiles of mean wind components and potential temperature and the calculated Ri profile in the nocturnal PBL under moderately stable conditions. [From Deardorff (1978); after Izumi and Barad (1963).]

in Ri. The Ri profile indicates that continuous turbulence may be expected only in the lower half of the SBL, where $Ri < 0.25$.

The sporadic turbulence regime is more common in the SBL over land. The typical observed profiles of U, V, Θ, and Ri in the very stable regime are shown in Figure 6.8. Note that both the wind components attain maximum values at low levels. The PBL depth based on the maximum in the wind speed profile is only about half of the depth of the surface inversion layer. The Ri profile indicates that the layer of possible continuous turbulence in which $Ri < 0.25$ is very shallow indeed and in the bulk of the SBL turbulence is likely to be intermittent, patchy, and weak.

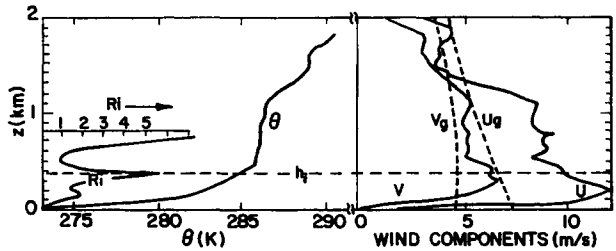

Figure 6.8 Observed wind and potential temperature profiles under very stable (sporadic turbulence) conditions at night during the Wangara Experiment. [From Deardorff (1978).]

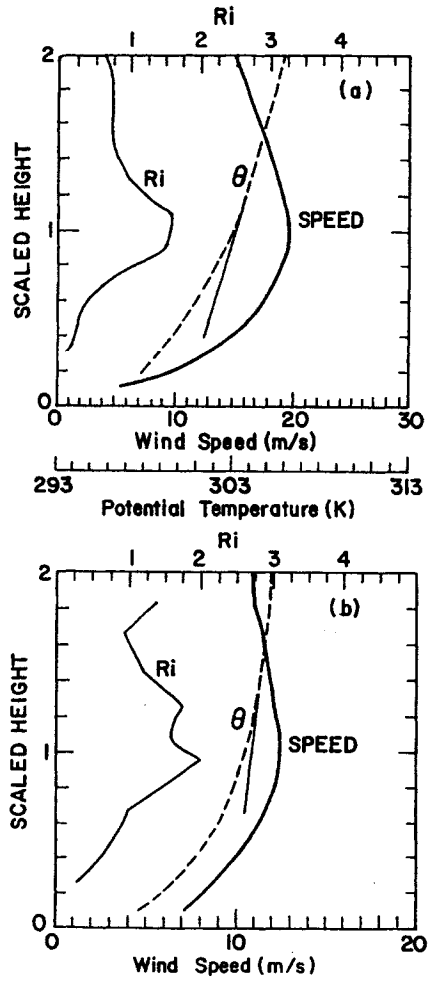

Figure 6.9 Composite profiles of wind speed, potential temperature and Richardson number scaled with respect to the low-level jet height at (a) O'Neill, Nebraska, during the Great Plains Experiment and (b) Hay, Australia, during the Wangara Experiment. [After Mahrt *et al.* Copyright © (1979) by D. Reidel Publishing Company. Reprinted by permission.]

The occurrence of a low-level jet is a common phenomenon in the SBL (Figure 6.9). The jet can become highly intensified when thermal or slope winds oppose the surface geostrophic wind. Such intensified low-level jets have frequently been observed over the Great Plains region of the United States. Figure 6.9 shows low-level jets in the composite wind speed profiles obtained

from observations during the Wangara Experiment (Clark *et al.*, 1971) and the Great Plains Field Program (Lettau and Davidson, 1957).

Other characteristic features of the stably stratified PBL are large directional shear (wind veering) and small PBL depth, both of which are manifestations of the effects of stability. The veering of wind with height is better illustrated through a representation of wind components in the form of a wind hodograph, which is the locus of the end points of velocity vectors at various heights. Figure 6.10 presents such hodographs from a 32 m tower at Plateau Station, Antarctica. These are actually averages of many observed wind profiles grouped under eight stability classes (from the least stable class 1 to the most stable class 8) and three periods or seasons. The corresponding temperature profiles have already been given in Figure 5.5. Note that with increasing stability, wind veering with height also increases. For extremely stable classes changes in wind direction with height can be detected even at low levels of 1 or 2 m, so that the surface layer becomes very shallow under these conditions.

The close relationship between wind veering and stability or temperature lapse rate is further demonstrated by observations given in Figure 6.11. Note that wind veering increases with increasing stability (negative lapse rate); the negative values (backing of wind) under superadiabatic conditions are probably due to the influence of thermal winds.

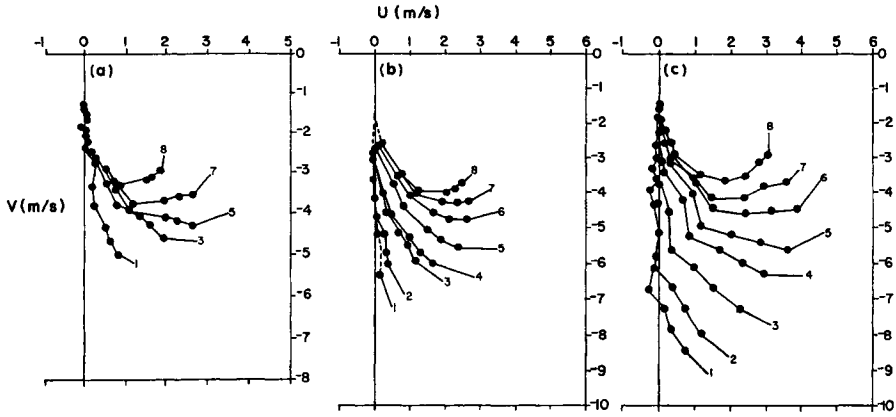

Figure 6.10 Averaged observed wind hodographs at Plateau Station, Antarctica, for (a) sunlight, (b) transitional, and (c) dark periods, grouped under different stability classes 1–8. Dots indicate ends of wind vectors at heights of 0.5, 1, 2, 4, 8, 12, 16, 20, 24, and 32 m. The components shown are in the so-called geotriptic coordinate system. [After Lettau *et al.* (1977).]

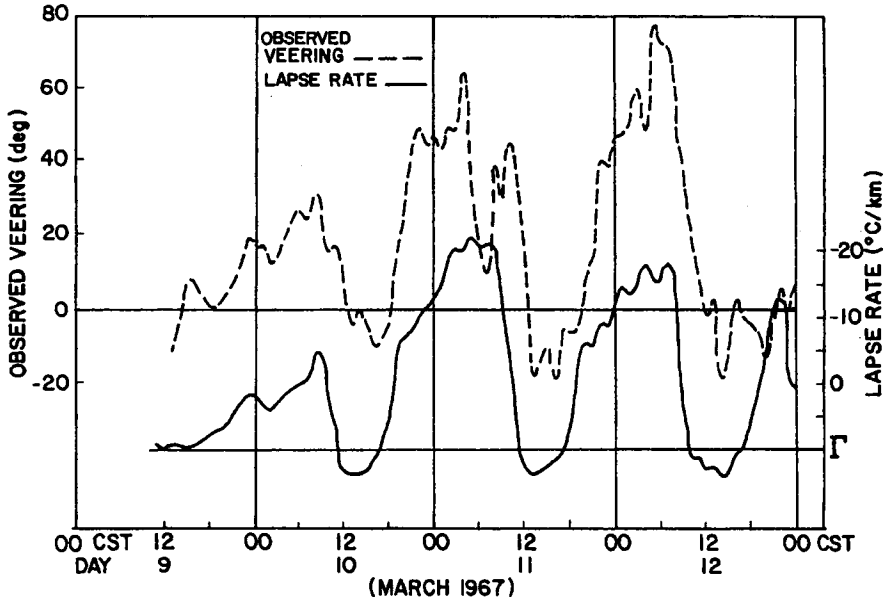

Figure 6.11 Observed relationship between wind veering (– – –) and lapse rate (——) near Oklahoma City. [After Gray and Mendenhall (1973).]

6.6 Diurnal Variations

Diurnal variations of wind speed and wind direction in the PBL have been inferred from observations collected at different locations. The evaluation of wind profiles in the course of a diurnal cycle may show large day-to-day variations due to changes in the synoptic weather situation and the surface energy balance. When averaged over long periods of time (order of a month or longer), however, the diurnal variations are better discerned.

Figure 6.12 shows the diurnal variations of mean wind speed (averaged over a period of 1 year) observed from an instrumented 500 m tower near Oklahoma City, Oklahoma. The range of times of sunrise and sunset, as well as the observation heights, are indicated in the figure. Note that the near-surface wind speed increases sharply after sunrise, attains a broad maximum in early afternoon, and decreases sharply near sunset. The diurnal wave at the higher level in the surface layer is similar, but with a reduced amplitude. The increase in the strength of surface winds following the morning inversion breakup is due to more rapid and efficient transfer of momentum from aloft through the evolving unstable or convective PBL in the daytime.

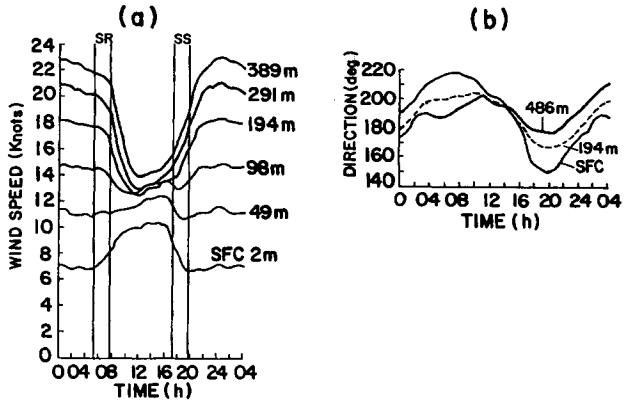

Figure 6.12 Diurnal variations of (a) mean wind speed and (b) mean wind direction, on an annual basis, for various height levels in the PBL near Oklahoma City, Oklahoma. [After Crawford and Hudson (1973).]

Above the surface layer, the diurnal wave becomes nearly 180° out of phase and wind speed decreases sharply following sunrise, attains a minimum value around noon, and increases in the afternoon and evening hours. The amplitude of the wave increases with height and attains its maximum value somewhere in the middle of the convective PBL. Although these observations did not extend to higher levels, the amplitude of diurnal variation of wind speed is expected to decrease farther up and vanish at the maximum height of the daytime PBL. Similar diurnal patterns of wind speed at various heights in the PBL are shown in Figure 6.13, which is based on 40-day averages of pibal observed winds during the Wangara expedition at a smooth rural site in Australia.

It can be inferred from the diurnal evolution of potential temperature and specific humidity profiles shown in Chapter 5 and, to some extent, from the wind profiles also, that PBL depth has a strong diurnal variation, especially during the daytime under clear skies. The unstable or convective PBL is usually capped by an inversion and the height of the inversion base z_i is considered to be a measure of the PBL depth h (actually, h is 5–30% larger than z_i, if one includes the interfacial transition layer in the former). The diurnal evolution of the height of the lowest inversion base on a typical day during the 1973 Minnesota experiment is shown in Figure 6.14. Also represented in the same figure is the diurnal variation of the surface heat flux H_0 whose cumulative input (integration with respect to time) to the PBL is primarily responsible for the growth of z_i or h.

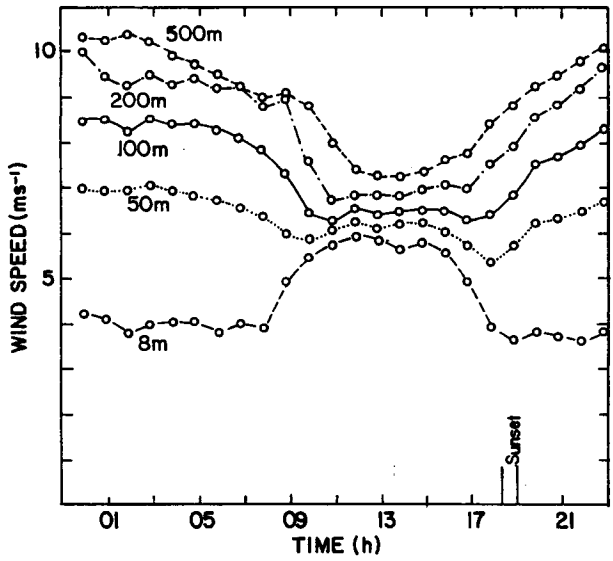

Figure 6.13 Diurnal variations of 40-day-averaged wind speeds at various heights in the PBL during the Wangara Experiment. [After Mahrt (1981).]

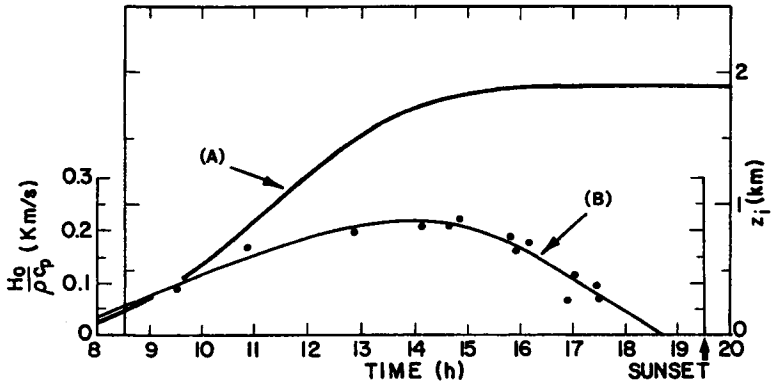

Figure 6.14 Typical variations of (A) the height of inversion base and (B) sensible heat flux during the daytime period in the Minnesota Experiment. [After Kaimal *et al.* (1976).]

6.7 Applications

The knowledge of wind distribution in the PBL has the following practical applications:

- Determining the rate of dissipation of the kinetic energy in the lower atmosphere.
- Determining local and regional transports of pollutants and air trajectories in the lower atmosphere.
- Estimating momentum flux or shear stress through the PBL and the surface drag.
- Estimating wind energy potential and designing wind power-generating systems.
- Designing tall buildings, towers, and bridges for wind loads.
- Designing wind shelters and other protective measures.

Problems and Exercises

1. Derive the thermal wind equations from the geostrophic wind relations, the hydrostatic equation, and the equation of state for the lower atmosphere, and indicate when and why the terms involving the vertical temperature gradient may be neglected.

2. Show that the net horizontal friction force per unit volume of a fluid element in the PBL is $\partial \boldsymbol{\tau}/\partial z$ and that it need not be opposite to the velocity vector $\mathbf{V}$. How is the friction force related to the ageostrophic wind vector?

3. The following measurements of mean winds and temperatures were made from the 200 m mast at Cabauw in The Netherlands on a September night:

Height (m)	Wind speed ($m\ s^{-1}$)	Wind direction (deg)	Temperature (°C)
5	2.2	194	8.58
10	2.7	194	8.81
20	3.5	202	9.08
40	5.4	217	10.15
80	8.2	234	12.19
120	9.1	240	12.96
160	8.7	246	12.86
200	7.8	250	12.63

Geostrophic wind speed at the surface $= 5.94\ m\ s^{-1}$
Geostrophic wind direction at the surface $= 263°$
Horizontal temperature gradient toward east $= -2.69 \times 10^{-5}\ K\ m^{-1}$
Horizontal temperature gradient toward north $= 8.85 \times 10^{-6}\ K\ m^{-1}$

Boundary layer depth = 100 m
Surface pressure = 1000 mbar

(a) Plot on a graph the wind speed, wind direction, and potential temperature profiles.
(b) Plot the wind hodograph, using the geographical coordinate system, and indicate geostrophic wind vectors at the surface and the top of the PBL. Compare the actual wind with the geostrophic wind at 100 m.
(c) Calculate and plot the wind component profiles, taking the x axis along the near-surface (5 m) wind.

4.
(a) Using the wind component and potential temperature profiles of the previous problem, determine the magnitudes of wind shear, potential temperature gradient, and Richardson number at the heights of 7.5, 15, 30, 60, 100, 140, and 180 m.
(b) Plot Ri as a function of height and indicate the probable top of the PBL based on the maximum in the Ri profile.

5. The following observations are for a midlatitude ($f = 10^{-4}\ s^{-1}$) PBL during the afternoon convective conditions:

Height[a] (m)	Wind speed[b] ($m\ s^{-1}$)	Wind direction[c] (deg)
1	7.7	311
32	11.0	315
61	11.4	315
610	11.7	321
1220	12.1	331

[a] PBL height = 1220 m.
[b] Surface geostrophic wind speed = 10.0 $m\ s^{-1}$.
[c] Surface geostrophic wind direction = 295°.

(a) Calculate the average magnitudes of geostrophic wind shear and the actual wind shear in the PBL, assuming geostrophic balance at the top of the PBL.
(b) Compute the total wind veering and frictional veering across the PBL, as well as the cross-isobar angle of the near-surface winds.
(c) Compute the pressure gradient, Coriolis, and friction forces per unit volume ($\rho = 1.2\ kg\ m^{-3}$) at the 610 m level and vectorially represent (to scale) the force balance at this level.

6. Calculate the magnitudes and directions of pressure gradient, Coriolis, and friction forces per unit mass of a fluid element at the top of a nocturnal surface layer where the actual winds are 7.07 m s^{-1} from the west, the geostrophic wind speed is 10 m s^{-1}, and the cross-isobar angle is 45° (take $f = 10^{-4}$ s^{-1}).